NASA TECHNICAL MEMORANDUM

NASA TM-78178

(N[illegible]A-TM-78178) SAMPLE STREAM DISTORTION MODELED IN CONTINUOUS-FLOW ELECTROPHORESIS (NASA) 46 p HC A03/MF A01 CSCL 07D

N80-13192

Unclas
G3/25 46237

SAMPLE STREAM DISTORTION MODELED IN CONTINUOUS-FLOW ELECTROPHORESIS

By P. H. Rhodes
Space Sciences Laboratory

August 1979

NASA

George C. Marshall Space Flight Center
Marshall Space Flight Center, Alabama

MSFC - Form 3190 (Rev June 1971)

TECHNICAL REPORT STANDARD TITLE PAGE

1. REPORT NO.	2. GOVERNMENT ACCESSION NO.	3. RECIPIENT'S CATALOG NO.
NASA TM-78178		

4. TITLE AND SUBTITLE	5. REPORT DATE
Sample Stream Distortion Modeled in Continuous-Flow Electrophoresis	August 1979
	6. PERFORMING ORGANIZATION CODE
7. AUTHOR(S) P. H. Rhodes	8. PERFORMING ORGANIZATION REPORT #
9. PERFORMING ORGANIZATION NAME AND ADDRESS George C. Marshall Space Flight Center Marshall Space Flight Center, Alabama 35812	10. WORK UNIT NO.
	11. CONTRACT OR GRANT NO.
	13. TYPE OF REPORT & PERIOD COVERED Technical Memorandum
12. SPONSORING AGENCY NAME AND ADDRESS National Aeronautics and Space Administration Washington, D.C. 20546	14. SPONSORING AGENCY CODE

15. SUPPLEMENTARY NOTES

Prepared by Space Sciences Laboratory, Science and Engineering

16. ABSTRACT

Buoyancy-induced disturbances in an electrophoresis-type chamber have been investigated. Five tracer streams (latex) were used to visualize the flows while a nine-thermistor array sensed the temperature field. The internal heating to the chamber was provided by a 400-Hz electrical field. Cooling to the chamber was provided on the front and back faces and, in addition, on both chamber side walls.

Disturbances to the symmetric base flow in the chamber occurred in the broad plane of the chamber and resulted from the formation of lateral and axial temperature gradients. The effect of these gradients was to retard or increase local flow velocities at different positions in the chamber cross section, which resulted in lateral secondary flows being induced in the broad plane of the chamber. As the adverse temperature gradients increased in magnitude, the critical Rayleigh number was approached and reverse (s rated) flow became apparent, which subsequently led to the onset of time variant secondary flows.

Further tests are planned to more completely delineate the temperature and velocity fields.

17. KEY WORDS	18. DISTRIBUTION STATEMENT
Electrophoresis Flow disturbances	Unclassified – Unlimited Gary H. Rhodes

19. SECURITY CLASSIF. (of this report)	20. SECURITY CLASSIF. (of this page)	21. NO. OF PAGES	22. PRICE
Unclassified	Unclassified	45	

For sale by National Technical Information Service, Springfield, Virginia 22151

TABLE OF CONTENTS

LIST OF ILLUSTRATIONS

LIST OF ILLUSTRATIONS (Concluded)

LIST OF TABLES

TECHNICAL MEMORANDUM

SAMPLE STREAM DISTORTION MODELED IN CONTINUOUS-FLOW ELECTROPHORESIS

I. INTRODUCTION

In 1976, S. Ostrach [1] developed a theory characterizing buoyancy-induced disturbances in an electrophoresis type flow chamber. His theory was based on the deformation of the parabolic flow profile in the narrow dimension of the chamber into a W-shaped profile. This phemonenon, which he showed to exist only in a downward flowing system, is induced by upward directed buoyancy flows. His solution to the problem of buoyancy-induced disturbances was then, obviously, to flow the chamber upward and inject the sample at the bottom of the chamber. In 1977 Semon [2] at General Electric tried the upward flowing scheme in a 5 mm thick chamber. His results failed to confirm Ostrach's theory in that the test results showed significant deformations at power levels an order of magnitude below Ostrach's predictions. In 1978 D. A. Saville [3] theoretically investigated buoyancy-induced flows in an electrophoresis type chamber. Saville gave several theories for the observed disturbances, among them Ostrach's, but could not resolve the discrepancy between Ostrach's theory and the General Electric experimental results.

It was this discrepancy between theory and experiment which served as the impetus for this effort, which has been done in concert with theoretical work underway by D. A. Saville and S. Ostrach. The experimental data were therefore generated for comparison to the work of Saville and Ostrach.

II. EXPERIMENTAL PROCEDURE

During the preceding 9 months, tests have been performed to investigate the effect of buoyancy-driven convective disturbances on flow in a 5 mm thick electrophoresis-type chamber. The many tests conducted (over 150) have allowed some preliminary deductions to be made concerning the various flows observed. The initially uniform flows are observed to be progressively deformed as a result of uneven heating of the buffer medium. Streams of particles injected into the flow are deflected and deformed as the power levels are increased until a state is reached where the sample streams no longer flow coherently through the chamber.

These observations have led to an explanation of buoyancy-induced disturbances in an electrophoresis-type chamber which has been supported, in part, by theoretical analysis. While the detailed delineation of the flow and temperature fields might change some of the analysis given below, it is believed that these preliminary observations should be disseminated for review and discussion.

The tests made to date were carried out in two phases. Phase I utilized flow visualization in the chamber together with external measurements of inlet buffer temperature, inlet cooling temperature, and buffer flow rate to characterize the observed flow disturbances. In phase II only one buffer flow rate was investigated; however, the flow characterization was augmented by temperature measurements in the chamber during each run. Many of the phenomena observed in phase I can be explained through the results of phase II, as will be shown.

Figure 1 shows the apparatus used in the phase I experiments. Buffer at temperature T_1 flows down into the 5 mm thick test chamber and is heated by a 400 Hz electrical field applied between two wire electrodes located at the chamber side walls. The 5 mm thick chamber was used to enhance the observation of the buoyancy-induced disturbances, while the ac electric field was used to eliminate any electrokinetic effects. Coolant entering at temperature T_2 flows up and dissipates heat from the front and rear chamber walls. Channels have been milled into the chamber side walls to allow coolant to flow up adjacent to the chamber side walls to control lateral temperature gradients. A tracer sample (latex) material is injected at various points to observe the flows taking place.

Each test consisted of increasing input power until the flow is disrupted. Here, disruption implies that a sample stream can no longer be followed through the chamber. The following conditions were maintained constant during each test:

a) The inlet buffer temperature T_1 (buffer entered the chamber at the top from the reservoir situated above the chamber).

b) The inlet coolant temperature T_2 (buffer entered the coolant passages of the bottom of the chamber).

c) The buffer and sample flow rate into the chamber.

A nominal equilibration time of 30 min was observed throughout the test runs until the onset of sample stream disintegration, at which time the test was terminated.

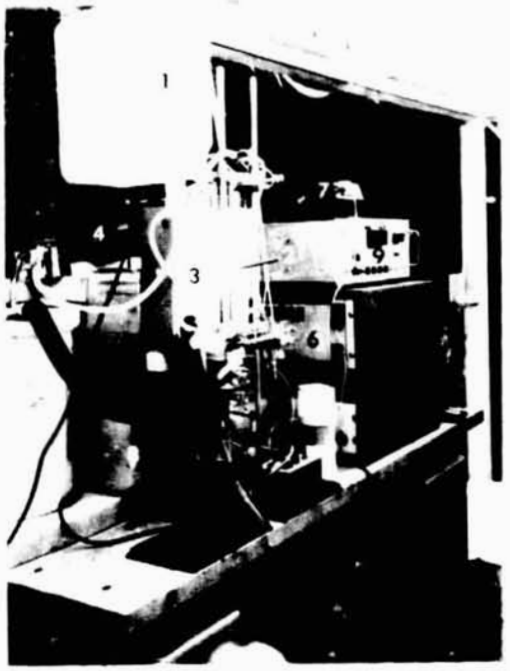

(a) EQUIPMENT SET-UP

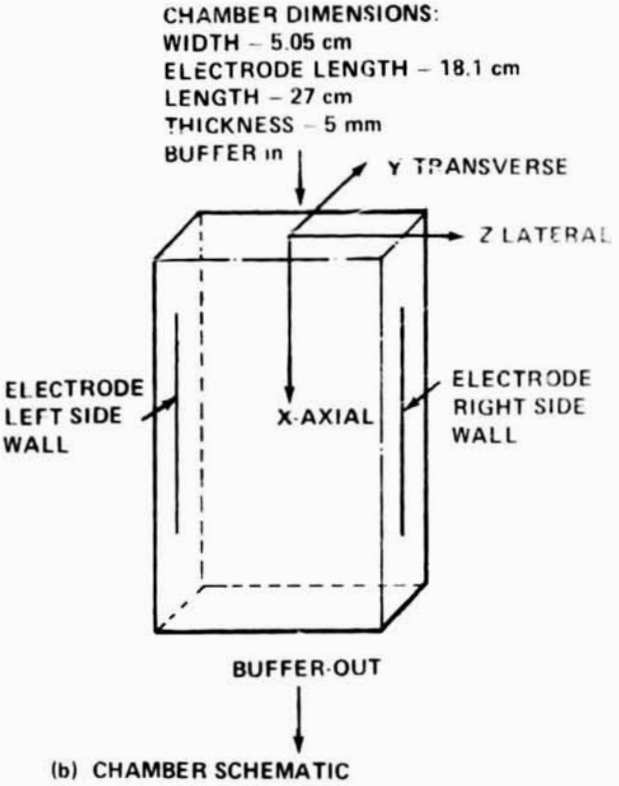

(b) CHAMBER SCHEMATIC

1. BUFFER RESERVOIR
2. FLOW CHAMBER
3. BACK LIGHT
4. SYRINGE PUMP
5. COOLER RESERVOIR
6. TEMPERATURE RECORDER
7. VOLTMETER
8. POWER SUPPLY
9. WATTMETER

Figure 1. Apparatus used in phase I experiments.

90 degrees about an axis perpendicular to the plane of the picture. The wire electrodes used in the phase I experiments were replaced by flat copper electrodes mounted on the inside chamber side walls. The methods of chamber cooling and a.c. heating remain the same as used in phase I.

III. PHASE I RESULTS

Phase I tests essentially consisted of increasing the power input at constant chamber flow conditions. An initially uniform, stable, flow condition was seen to progressively deteriorate through self-induced perturbations to the state of unstable flow. The perturbations characterized by deflection, meandering, distortion, and ribbon formation of the sample stream were evident before the onset of instability. These phenomena are shown respectively in Figures 3 through 6. While deflection, meandering and distortion of the sample stream might be expected, ribbon formation came as a surprise. As internal heating of the fluid takes place, the initially cylindrical sample stream cross section transforms into a rectangular shape which appears as a ribbon. The long axis of the rectangular cross section is perpendicular to the plane of the chamber faces, i.e., oriented in the transverse direction.

Figure 3. Typical stream deflection.

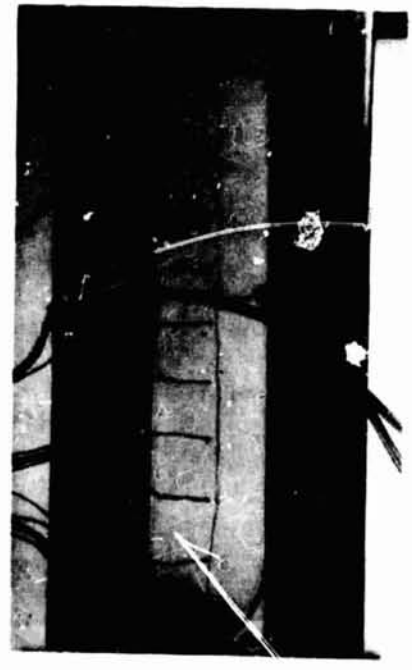

Figure 4. Typical stream meandering.

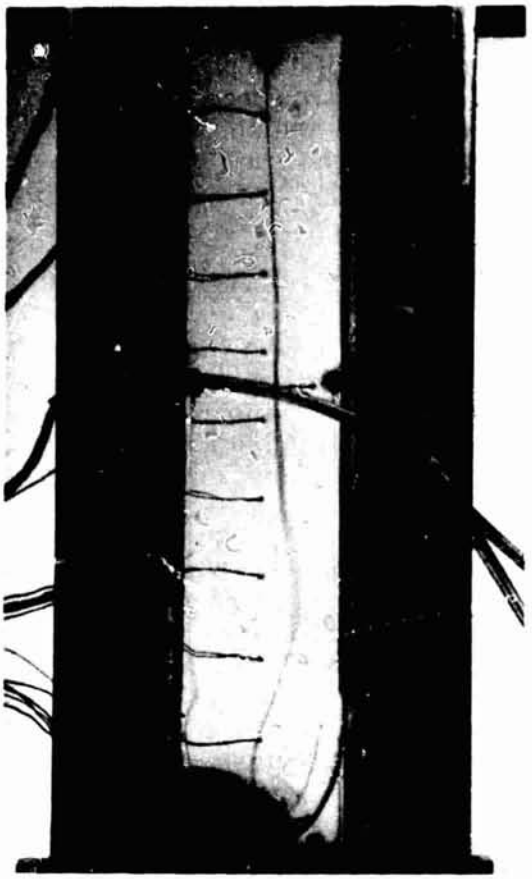

Figure 5. Typical stream distortion.

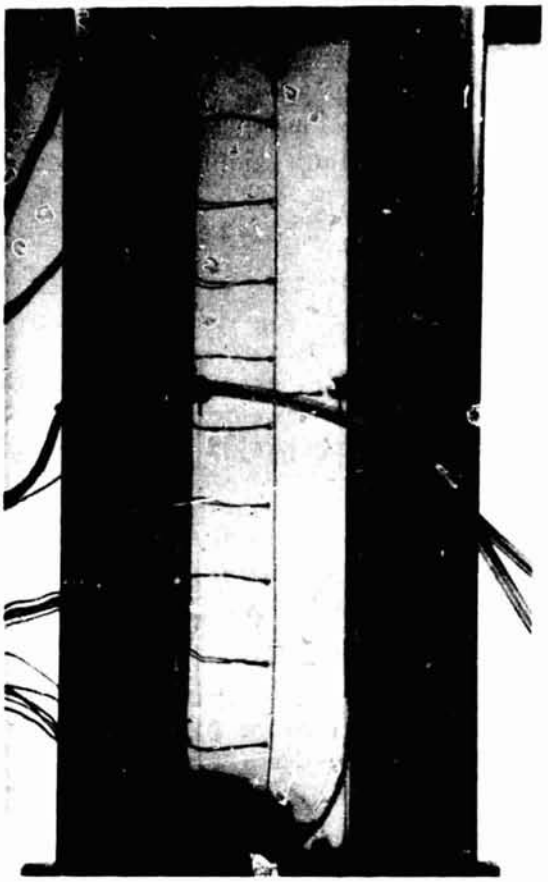

Figure 6. Typical stream ribbon formation.

It is recognized that the preceding perturbations would have precluded effective electrophoretic separation long before the onset of unstable flow; however, the limit of stability forms a reproducible criterion amenable to mathematical analysis which sets an upper bound for coherent flow in the chamber and, as such, is very useful in determining the origin of all flow perturbations in the chamber.

Figure 7 shows the limit of stability in the flow chamber for three buffer flow rates. Note that stability is enhanced by (a) increasing flow rate, (b) increasing axial temperature difference ΔT, and (c) decreasing chamber temperature by decreasing the coolant temperature T_2. Increasing the buffer flow rate effectively swamps out buoyancy-driven disturbances, thus contributing to flow stability; increasing the axial temperature difference ΔT reduces the probability for the occurrence of

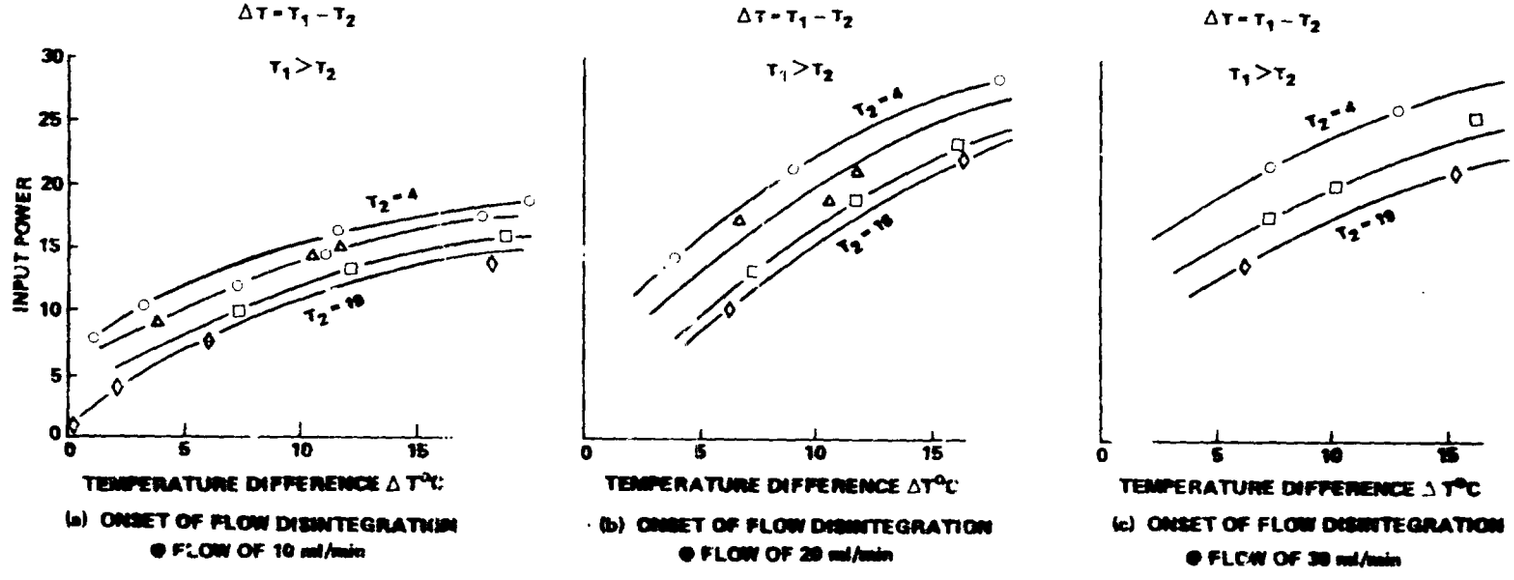

Figure 7. Limits of power input at the onset of unstable flow.

local unstable gradients resulting from nonuniform or ineffective cooling of the chamber; and finally, lowering the chamber temperature reduces the coefficient of thermal expansion which effectively reduces convective disturbances.

The effect of lateral temperature gradients is very important, as the following sequence of test results indicates. Figure 8 shows a steady flow situation with side wall cooling on both sides. Note the flow disturbance at the termination of the left electrode, which is due to insufficient cooling of the left side wall. The perturbation appears centered at the electrode termination. The main stream is deflected to the right because the flow is necessarily deflected away from the region of retarded flow on the left. Figure 9 shows the development of a disturbance pattern on the right side 3 min after side wall coolant flow was stopped on that side. The disturbance initially developed at the termination of the electrode and moved up as shown. Note deflection of the main stream to the left as a result of the induced flow obstruction. Figure 10 shows the development of a circulation pattern at the location of the

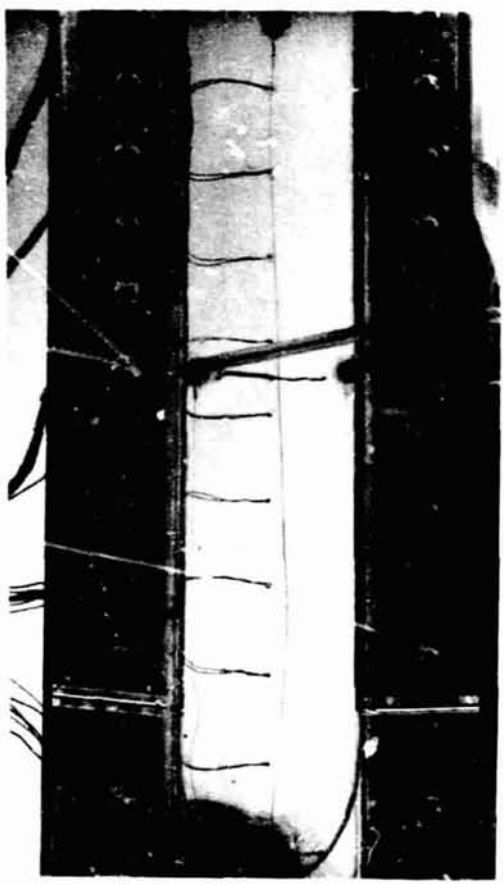

Figure 8. Flow with cooling both sides (arrow marks electrode termination).

Figure 9. Flow with cooling left side only.

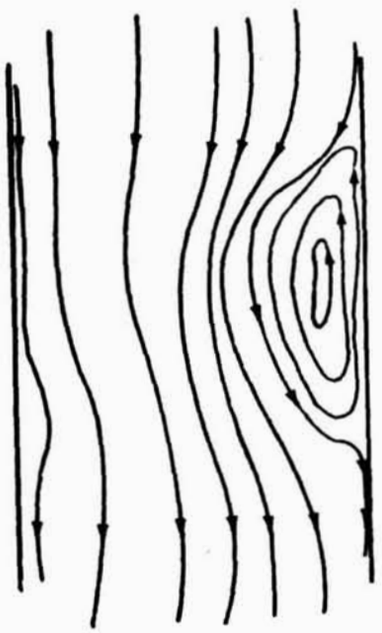

FLOW FIELD SCHEMATIC
FOR FIGURE 10

Figure 10. Flow with cooling left side only.

previously observed disturbance with the accompanying further deflection of the main stream. Figure 11 shows reestablishment of the initial flow situation 2 min after resumption of coolant flow in the right side wall. Figure 12 shows the flow configuration 6 min after clamping flow on the left side wall. Here again, the flow disturbance has developed into a circulation pattern which has caused the appropriate main stream deflection.

The previously mentioned ribbon formation is thought to be caused by the transverse temperature gradient producing upward directed buoyancy flows which blunt the parabolic velocity profile of the buffer flow through the chamber. The following experiment suggests that secondary flows in the chamber cross section cause the observed ribbon twists and deformation. Figure 13 shows an initially straight ribbon with a leak provided in the right sample inlet port. This leak should cause deflection of the stream by inducing a lateral flow in the chamber

Figure 11. Flow with cooling both sides.

Figure 12. Flow with cooling right side only.

cross section. Figure 14 shows the stream configuration 2 min after initiation of the leak. Note the deflection and twist of the ribbon which is apparently due to the induced cross flow in the chamber. Figure 15 shows the original straight ribbon reformed 4 min after plugging the leak.

Lateral temperature gradients initiate disturbances which subsequently lead to circulations; as preceding results indicate. It will be shown in the phase II results that adverse axial temperature gradients can also cause these types of disturbances.

As the power input to the system is increased, the circulations are enlarged so that they cover nearly the entire flow region (as Figures 16 and 17 indicate), subsequently destroying the stable axial temperature

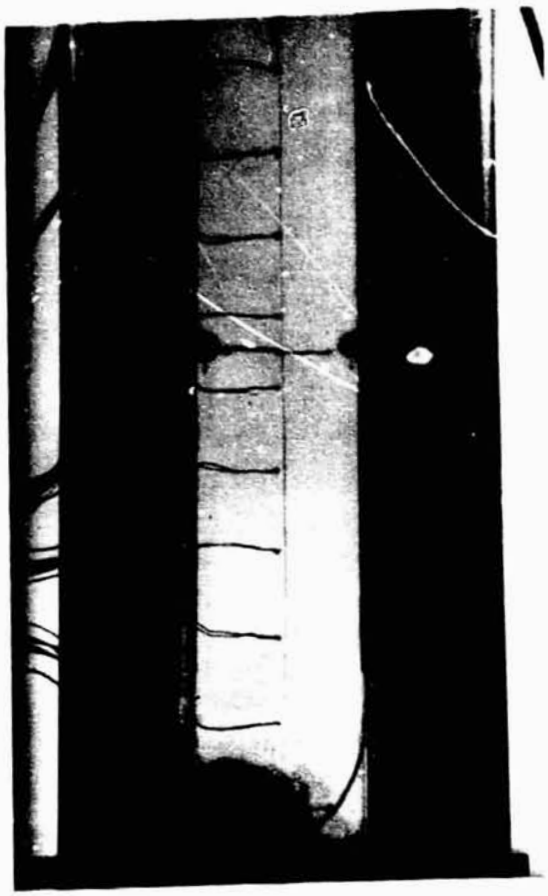

Figure 13. Flow at initiation of leak.

Figure 14. Flow with leak on right side.

gradient and leading to unstable convection, as shown in Figure 18. Indeed, the stable axial gradient apparently must be present to offset perturbations such as those produced by lateral gradients. It is possible that the lateral temperature gradient is a maximum at the termination of the electrode region which would explain the origin of the circulations discussed above. Some phase II results indicate that this is the case; for example, note the zero power temperature field discussion of case III.

IV. PHASE II RESULTS

Phase I described several observed flow perturbations which eventually lead to flow disruption. The phase II results will attempt to explain some of the observed flow phenomena in terms of the temperature field in the chamber. The figures depicting disturbed flows in the

Figure 15. Flow without leak.

Figure 16. Flow at power input 4.3 W, t = 0.

Figure 17. Flow at power input 4.3 W, t = 19 min.

Figure 18. Flow at power input 23.3 W.

phase II results will show stream deflections resulting from local velocity perturbations to the uniform base flow of the chamber. Some disturbances are therefore caused by slow flow regions which deflect the flow accordingly. The disturbances, in some cases, are subsequently transformed into circulation patterns, i.e., separated flow. The results will be presented in terms of three typical flow cases observed in the tests.

A. Case I – Flow Perturbations as a Function of Joule Heating

Figure 19 shows the phase II chamber configuration and the thermistor identification scheme, while Table 1 shows the thermistor locations in terms of the coordinate system shown in Figure 2. The flow shown is at zero power input with a buffer flow rate of 19 ml/min. The five sample streams flow evenly through the chamber. Note, in Table 2, the favorable temperature gradients throughout the system, depicting a stable flow system. Note that in Figure 19 the sample streams have also been labeled for easy reference.

TABLE 1. NOZZLE AND THERMISTOR LOCATIONS

Thermistor	Axial Distance (cm)	X	Lateral Distance (cm)	Z
1	4.6	0.25	0.28	1.12
2	9.2	0.51	0.28	1.12
3	13.8	0.76	0.28	1.12
4	18.4	1.02	0.28	1.12
5	23.1	1.28	0.28	1.12
6	12.8	0.71	2.1	8.4
7	23.1	1.28	-2.2	-8.8
8	12.8	0.71	-2.2	-8.8
9	23.1	1.28	2.1	8.4
(a) Thermistor locations				
Injection Nozzle Label	Axial Distance (cm)	X	Lateral Distance (cm)	Z
"a"	4.3	0.24	-2.0	-8.0
"b"	4.4	0.24	-1.0	-4.0
"c"	4.4	0.24	0	0
"d"	4.4	0.24	1.0	4.0
"e"	4.4	0.24	2.0	8.0
(b) Nozzle locations				

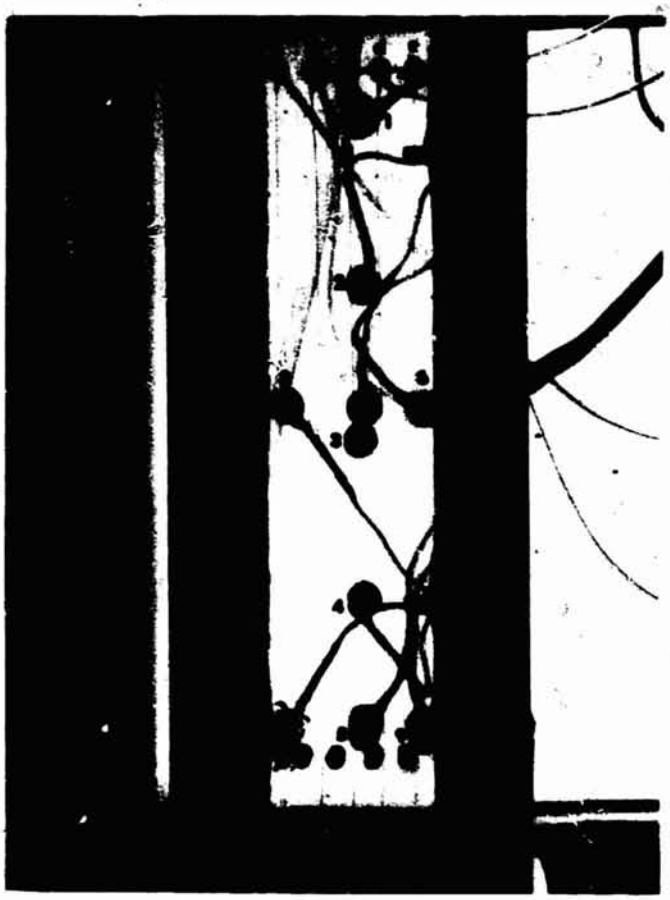

Figure 19. Phase II test chamber with thermistor locations.

TABLE 2. CHAMBER TEMPERATURES AND TEST PARAMETERS FOR FIGURE 19

Temperatures (°C)			Transverse Temperature Differences (°C)	Lateral/Axial ΔT (°C)			
Position	Wall	Center Plane		Span	Wall	Center Plane	Chamber Parameters
1	19.76	20.97	1.07	1-2	1.11	1.41	T_1 22.1°C
2	18.66	19.57	0.8	2-3	1.07	1.07	T_2^1 15.4°C
3	17.62	18.53	0.73	3-8	0.15	0.32	T_3^2 16.2°C
4	17.17	17.77	0.42	3-6	0.17	0.12	
5	16.68	17.31	0.47	3-4	0.4	0.71	Power: 0 W
6	17.44	18.41	0.71	4-5	0.53	0.5	Flow: 19 ml/min
7	16.26	16.69	0.28	5-7	0.42	0.63	Re no.: 3.1
8	17.47	16.91	0.5	5-9	0.42	0.35	Gr no.: 30.3
9	16.27	16.96	0.51				Ra no.: 0

All chamber temperatures will be given as in Table 2. The sequence for obtaining the temperature is: first, wall temperatures are taken sequentially; second, wall and center plane temperatures are taken sequentially as each thermistor is moved to the center plane to obtain the transverse temperature differences; and, finally, the center plane temperatures are taken sequentially. The temperatures are calculated according to a calibration curve fit of the output voltages of the thermistors. The temperature differences, however, are calculated with respect to the voltage differences in order to reduce curve fitting error. The above procedure has been verified to be accurate to ±0.05°C. Slight discrepancies will be found between the temperatures and the temperature differences due to the curve fit error involved and also due to the sequential method of taking data which was used.

Figure 20 shows the flow configuration at a power input of 4.66 W and a buffer flow rate of 20 ml/min. Note the deflection of sample streams c, d, and e to the right and a and b to the left occurring in the vicinity of thermistor 4. The results of phase I would suggest that a disturbance is beginning to develop at the top of the chamber and near thermistor 4. Table 3 shows the temperature field associated with this flow situation.

Note first the sizable decrease in axial gradient at the top of the chamber, ΔT_{1-2}. This is the expected unstable end of the chamber. Streams b and d are deformed inward, indicating the presence of two disturbances on either side of the chamber between thermistors 1 and 2. Note also the adverse axial gradient ΔT_{3-4} beginning to develop. This correlates with the disturbance in the vicinity of thermistor 4 previously mentioned.

Figure 21 shows the flow configuration at a power input of 6.82 W. The disturbances previously observed have increased in size and ribbons have been formed with twists. The flow, however deformed, is still quite stable.

Table 4 shows the continual degradation of the stable axial gradient at the top of the chamber, i.e., ΔT_{1-2}. The unstable gradient between thermistors 3 and 4 (ΔT_{3-4}) is also increased, which is in agreement with the observed enlarged disturbances.

Figure 22 shows the flow at a power input of 8.00 W. Note that the disturbances on the left side of the chamber have enlarged and together confine flow to the right side of the chamber cross section. Observe that stream b is breaking up in the region between thermistors 4 and 7 and clearly shows a circulation pattern beginning to develop.

Table 5 shows the temperatures present at the termination of the run. Note the negative gradients in the vicinity of the observed circulation patterns and the general approach to zero for gradients at the

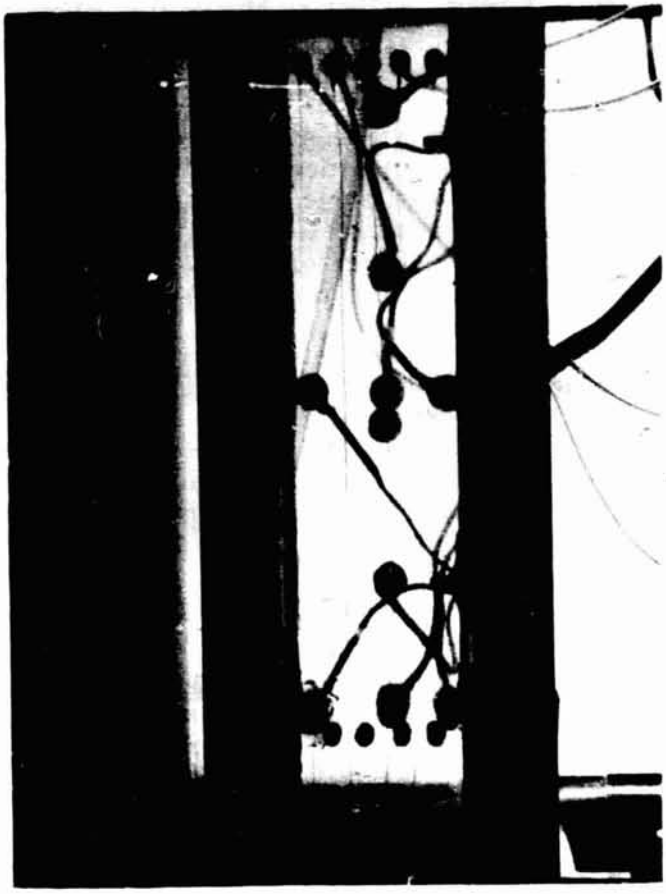

Figure 20. Flow at power input of 4.66 W.

TABLE 3. CHAMBER TEMPERATURES AND TEST PARAMETERS FOR FIGURE 20

Temperatures (°C)			Transverse Temperature Difference (°C)	Lateral/Axial ΔT (°C)			Chamber Parameters
Position	Wall	Center Plane		Span	Wall	Center Plane	
1	20.62	21.68	0.95	1-2	0.37	0.44	T_1 22.3°C
2	20.26	21.25	0.78	2-3	0.7	0.6	T_2 16°C
3	19.59	20.67	1.09	3-8	0.3	0.25	T_3 16.6°C
4	19.59	20.35	0.72	3-6	0.26	0.21	
5	18.86	19.87	0.95	3-4	-0.04	0.28	Power: 4.66 W
6	19.32	20.45	1.05	4-5	0.76	0.51	Flow: 20 ml/min
7	18.42	19.13	0.7	5-7	0.44	0.74	Re no.: 3.3
8	19.29	20.4	0.54	5-9	0.48	0.43	Gr no.: 32.5
9	18.38	19.44	0.99				Ra no.: 0.6

Figure 21. Flow at power input of 6.82 W.

TABLE 4. CHAMBER TEMPERATURES AND TEST PARAMETERS FOR FIGURE 21

Temperatures (°C)			Transverse Temperature Differences (°C)	Lateral/Axial ΔT (°C)			Chamber Parameters
Position	Wall	Center Plane		Span	Wall	Center Plane	
1	20.86	21.92	1.05	1-2	0.04	0.06	T_1 22.5°C
2	20.83	21.82	1.03	2-3	0.54	0.28	T_2 16.1°C
3	20.31	21.54	1.18	3-8	0.16	0.25	T_3 16.8°C
4	20.45	21.51	1.02	3-6	0.2	0.3	
5	19.7	20.95	1.19	3-4	-0.17	-0.01	Power: 6.82 W
6	20.11	21.23	1.1	4-5	0.78	0.58	Flow: 20 ml/min
7	19.26	20.08	0.83	5-7	0.44	0.87	Re no.: 3.3
8	20.16	21.31	1.13	5-9	0.61	0.48	Gr no.: 39.1
9	19.09	20.47	1.32				Ra no.: 1.6

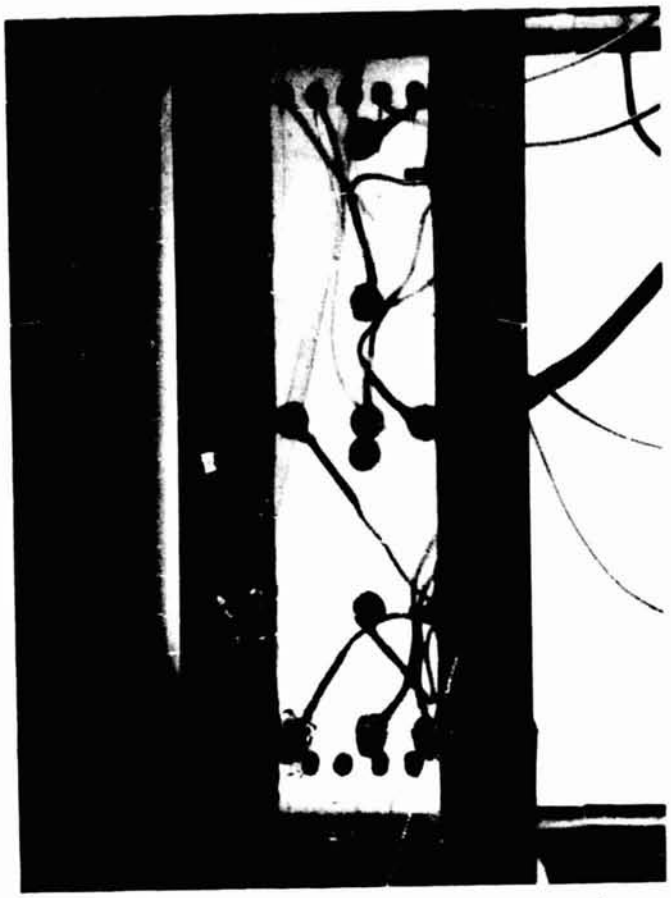

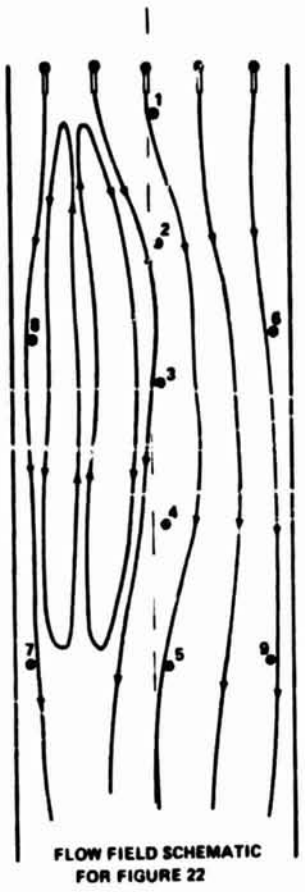

FLOW FIELD SCHEMATIC
FOR FIGURE 22

Figure 22. Flow at power input of 8.00 W.

TABLE 5. CHAMBER TEMPERATURES AND TEST PARAMETERS FOR FIGURE 22

Temperatures (°C)			Transverse Temperature Differences (°C)	Lateral/Axial [illegible] (°C)			Chamber Parameters
Position	Wall	Center Plane		Span	Wall	Center Plane	
1	21.03	22.05	0.98	1-2	-0.1	-0.1	T_1 22.6°C
2	21.13	22.14	0.93	2-3	0.54	0.15	T_2 16.1°C
3	20.6	22	1.36	3-8	-0.01	0.05	T_3 16.8°C
4	21.09	22.11	0.96	3-6	0.05	0.21	
5	19.95	21.56	1.45	3-4	-0.51	-0.13	Power: 8 W
6	20.54	21.77	1.13	4-5	1.15	0.58	Flow: 20 ml/min
7	19.73	20.64	0.9	5-7	0.22	0.91	Re no.: 3.3
8	20.62	22.05	1.43	5-9	0.54	0.51	Gr no.: 48.4
9	19.42	19.42	0.9				Ra no.: 5.7

center plane. Therefore, in this run we have seen a general decline in favorable gradients as the disturbance patterns were developed through increased heating in the chamber.

A second run is now described to verify the results shown for the previous run. Figure 23 and Table 6 show, respectively, the zero power flow configuration and chamber temperatures. Note the large stable axial gradients at the top of the chamber and the uniform flow in the chamber.

Figure 24 shows the flow configuration at a power input of 7.70 W. Note the deflection of the sample streams to the right, indicating the development of disturbances (flow retardations) on the left side of the chamber. Also observe the ribbon formations; sample stream b exhibits an undeformed ribbon while the ribbon of stream c is twisted. As shown in the phase I leak experiments, this condition implies the existence of secondary flows in the chamber cross section. Table 7 shows the temperatures present in the chamber. Note the large decline in favorable gradient at the top of the chamber when compared to the zero power condition.

Figure 25 shows the flow at a power input of 12.00 W. Two deflection patterns can be seen at the top of the chamber, while a third and larger disturbance is seen on the left side between thermistors 3 and 4. The sample streams have also been spread into rather large ribbons. Note the elevated power level obtainable for this run as compared to a maximum power input of 7.7 W for the first run. This is due to the differences in buffer inlet and coolant inlet temperatures for the respective runs, which provide a larger stabilizing axial gradient for the second run. This is in agreement with the results shown in Figure 7.

Table 8 shows that adverse axial gradients exist in the vicinity of the observed disturbances.

Therefore, while the flow is still stable, large disturbance patterns have been developed which transform the initial uniform flow into deflected and distorted streams which, nevertheless, are seen to be steady state phenomena. Meandering, however, has been observed to be a transient phenomena occurring and apparently being initiated by the development or decay of the observed disturbance patterns.

A final run will now be shown in which the disturbance patterns described previously occur in a striking fashion due to a smaller imposed axial gradient. Figure 26 shows the stable zero power flow configuration, while Table 9 shows the associated temperatures.

Note the reduced favorable gradients due to the smaller overall axial gradient. Indeed, a slight adverse lateral gradient exists between thermistors 3 and 8.

Figure 23. Flow at zero power input.

TABLE 6. CHAMBER TEMPERATURES AND TEST PARAMETERS FOR FIGURE 23

Temperatures (°C)			Transverse Temperature Differences (°C)	Lateral/Axial ΔT (°C)			Chamber Parameters
Position	Wall	Center Plane		Span	Wall	Center Plane	
1	19.11	20.64	1.54	1-2	2.12	2.47	T_1 23°C
2	17	18.17	1.23	2-3	1.84	1.94	T_2 10.7°C
3	15.2	16.26	1.12	3-8	0.26	0.28	T_3 12°C
4	14.37	14.95	0.7	3-6	0.26	0.04	
5	13.43	14.09	0.82	3-4	0.79	1.27	Power: 0 W
6	14.94	16.23	1.37	4-5	0.99	0.91	Flow: 19 ml/min
7	12.65	13.02	0.49	5-7	0.78	1.07	Re no.: 2.8
8	14.95	15.99	1.06	5-9	0.7	0.59	Gr no.: 30.6
9	12.73	13.5	0.9				Ra no.: 0

Figure 24. Flow at power input of 7.70 W.

TABLE 7. CHAMBER TEMPERATURES AND TEST PARAMETERS FOR FIGURE 24

Temperatures (°C)			Transverse Temperature Differences (°C)	Lateral Axial ΔT (°C)			Chamber Parameters
Position	Wall	Center Plane		Span	Wall	Center Plane	
1	19.75	21.48	1.64	1-2	0.7	0.87	T_1 23.1°C
2	19.06	20.62	1.49	2-3	1.45	1.23	T_2 11°C
3	17.64	19.12	1.69	3-8	0.15	0.1	T_3 12.3°C
4	17.36	18.74	1.28	3-6	0.27	0.12	
5	16.11	18.04	1.63	3-4	0.24	0.64	Power: 7.7 W
6	17.37	19.29	1.82	4-5	1.29	0.74	Flow: 20.5 ml/min
7	15.42	16.65	1.17	5-7	0.69	1.38	Re no.: 3.4
8	17.5	19.3	1.8	5-9	0.97	0.75	Gr no.: 48.6
9	15.14	17.29	2.06				Ra no.: 0

Figure 25 Flow at power input of 12.00 W.

TABLE 8. CHAMBER TEMPERATURES AND TEST PARAMETERS FOR FIGURE 25

Temperatures (°C)			Transverse Temperature Differences (°C)	Lateral/Axial ΔT (°C)			Chamber Parameters
Position	Wall	Center Plane		Span	Wall	Center Plane	
1	20.08	21.88	1.73	1-2	-0.15	0.1	T_1 23.3°C
2	20.24	21.79	1.47	2-3	1.28	0.66	T_2 11.3°C
3	18.98	21.15	2.06	3-8	0.15	0.25	T_3 12.6°C
4	19.52	20.97	1.33	3-6	0.1	0.21	
5	17.93	19.78	1.72	3-4	-0.59	0.15	Power: 12 W
6	18.84	20.93	1.95	4-5	1.62	1.21	Flow: 20 ml/min
7	17.04	18.63	1.46	5-7	0.89	1.15	Re no.: 3.3
8	18.8	20.9	2.1	5-9	1.26	0.47	Gr no.: 64.4
9	16.66	19.31	2.54				Ra no.: 3.7

Figure 26. Flow at zero power input.

TABLE 9. CHAMBER TEMPERATURES AND TEST PARAMETERS FOR FIGURE 26

Temperatures (°C)			Transverse Temperature Differences (°C)	Lateral/Axial ΔT (°C)			
Position	Wall	Center Plane		Span	Wall	Center Plane	Chamber Parameters
1	18.81	19.66	0.74	1-2	1.1	1.06	T_1 20.3°C
2	17.7	18.63	0.9	2-3	0.45	0.6	T_2 16°C
3	17.26	18.03	0.59	3-8	-0.1	0.2	T_3 16.7°C
4	17	17.52	0.35	3-6	0.04	0.14	
5	16.77	17.27	0.26	3-4	0.22	0.48	Power: 0 W
6	17.19	17.86	0.48	4-5	0.24	0.28	Flow: 20 ml/min
7	16.46	16.77	0.11	5-7	0.3	0.45	Re no.: 3.3
8	17.35	17.8	0.28	5-8	0.29	0.22	Gr no.: 25
9	16.48	17	0.27				Ra no.: 0

Figure 27 shows two well-developed disturbances in the chamber which combine to route flow through the chamber as shown. The flow schematic shows the probable circulations present; indeed, a faint trace of the upper left circulation can be seen in the photograph. Again, adverse axial gradients appear in the regions of circulation, as Table 10 shows; also, an adverse lateral wall gradient exists in the vicinity of thermistor 3.

It is interesting to observe that the adverse lateral gradient is in the region of circulation, while the stable lateral gradient (to the left of 3) is in a region of axial flow. The relationship between lateral and axial temperature gradients will be discussed further in the following case.

B. Case II – Effect of Lateral Gradients

The following series of tests investigated the effect of lateral gradients induced by shutoff of the side wall cooling. First, a uniform flow situation was initiated at a moderate power level; then one side wall flow was shut off, and the results were observed and comparison made with the initial flow condition.

Figure 28 shows the uniform initial flow situation with a power input of 5.7 W. The slight deflection of stream b indicates that small disturbances might be present. Table 11 shows the temperatures associated with this flow.

Figure 29 shows two disturbances which developed at the left side wall 3.5 min after coolant to that side was shut off. These are typical of those observed in the phase I tests and appear to initiate at the side wall near the termination of the electrode. Table 12 shows the associated temperatures.

Note the increased adverse lateral gradient between thermistors 3 and 8 and the decrease in stable gradient between 5 and 7, as expected with the left side coolant off. It is obvious that these lateral gradients initiate the observed disturbances; however, it is not clear why they occur at the electrode terminations. The high thermal conductivity of the electrode itself could cause high local lateral gradients at the electrode terminations. When disturbances occur, there must be an interaction between the local axial and lateral gradients due to the convective process. This is seen by comparing Table 11 to Table 12 with respect to the axial and lateral gradients. This relationship is, however, shown much more distinctly in the following case of zero power runs.

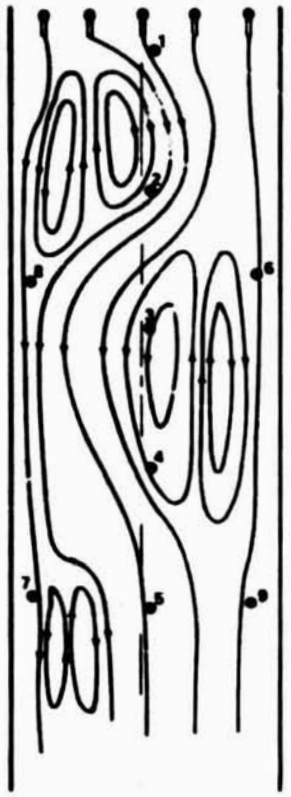

FLOW FIELD SCHEMATIC
FOR FIGURE 27

Figure 27. Flow at power input of 7.52 W.

TABLE 10. CHAMBER TEMPERATURES AND TEST PARAMETERS FOR FIGURE 27

Temperatures (°C)			Transverse Temperature Differences (°C)	Lateral/Axial ΔT (°C)			Chamber Parameters
Position	Wall	Center Plane		Span	Wall	Center Plane	
1	20.22	20.36	0.91	1-2	-0.05	-0.55	T_1 20.4°C
2	20.3	21.06	0.76	2-3	0.07	-0.11	T_2 16.2°C
3	19.7	21.14	1.51	3-8	0.18	0.97	T_3 16.9°C
4	20.07	20.89	1.02	3-6	-0.52	0.09	
5	19.45	20.44	0.98	3-4	-0.4	0.22	Power: 7.52 W
6	20.2	21.03	0.85	4-5	0.65	0.47	Flow: 20 ml/min
7	18.82	19.84	0.87	5-7	0.62	0.63	Re no.: 3.3
8	19.51	20.16	0.62	5-9	0.67	0.44	Gr no.: 48.4
9	18.77	19.99	1.11				Ra no.: 5.3

Figure 28. Flow with both side walls cooled, 5.70 W.

TABLE 11. CHAMBER TEMPERATURES AND TEST PARAMETERS FOR FIGURE 28

Temperatures (°C)			Transverse Temperature Differences (°C)	Lateral/Axial ΔT (°C)			
Position	Wall	Center Plane		Span	Wall	Center Plane	Chamber Parameters
1	19.37	20.14	0.74	1-2	0.27	0.1	T_1 20.8°C
2	19.1	20.01	0.9	2-3	0.52	0.25	T_2 15.4°C
3	18.54	19.76	1.29	3-8	-0.2	0.46	T_3 16.2°C
4	18.79	19.54	0.84	3-6	-0.33	-0.07	
5	18.23	19.12	0.95	3-4	-0.29	0.18	Power: 5.7 W
6	18.85	19.8	0.96	4-5	0.59	0.45	Flow: 18 ml/min
7	17.94	18.48	0.63	5-7	0.3	0.64	Re no.: 3
8	18.74	19.29	0.6	5-9	0.54	0.37	Gr no.: 41.3
9	17.69	18.75	1.15				Ra no.: 3.4

Figure 29. Flow with left cooling shut off, 5.70 W.

TABLE 12. CHAMBER TEMPERATURES AND TEST PARAMETERS FOR FIGURE 29

Temperatures (°C)			Transverse Temperature Differences (°C)	Lateral/Axial ΔT (°C)			
Position	Wall	Center Plane		Span	Wall	Center Plane	Chamber Parameters
1	19.4	20.28	0.81	1-2	0.1	0.02	T_1 20.8°C
2	19.3	20.25	0.9	2-3	0.6	0.2	T_2 15.8°C
3	18.72	20.04	1.22	3-8	-0.57	-0.14	T_3 16.5°C
4	19.07	19.92	0.76	3-6	-0.33	0.03	
5	18.61	19.55	0.83	3-4	-0.38	0.09	Power: 5.7 W
6	19.02	19.98	0.88	4-5	0.49	0.39	Flow: 18 ml/min
7	18.5	19.48	0.88	5-7	0.1	0.07	Re no.: 3
8	19.28	20.17	0.75	5-9	0.71	0.35	Gr no.: 37.6
9	17.9	19.2	1.19				Ra no.: 2.4

C. Case III – Zero Power Instability

To further investigate chamber stability, the following test sequence was devised:

a) The coolant exit temperature T_3 was set slightly below the buffer inlet temperature T_1 to produce a uniform, stable configuration.

b) The coolant temperature was then allowed to rise slowly so that an unstable flow condition at zero power would be approached, while

c) The temperature and flow conditions were monitored to provide information on the mechanism of flow disruption.

Figure 30 shows a uniform stable flow situation despite the adverse wall temperature gradients and the essentially neutral center plane gradients shown in Table 13.

Figure 31 shows two disturbance patterns forming near the top of the chamber with up-flow (separation) being initiated at the upper left (chamber) side wall. Figure 32 shows the flow situation 1 min later with the up-flow moving into the top of the chamber. The temperatures associated with this configuration are given in Table 14. The disturbances appear in the region of the chamber where adverse axial temperature gradients exist, although sizeable adverse lateral gradients are probably there also (not shown due to inadequate thermistor coverage), as indicated by ΔT_{3-6} and ΔT_{3-8}.

Figure 33 shows well-developed circulations in the chamber with only stream c flowing directly through the chamber. Circulation pairs which rotate in opposite directions are seen to be located on each side of stream c near the middle of the chamber. Table 15 shows the rather large adverse lateral gradients which are probably responsible for these observed circulations.

Figure 34 shows a final state of apparently chaotic flow; however, careful observation will reveal two large circulation patterns on each side of the chamber while the streams from ports d and e execute a tortuous route through the chamber. Table 16 shows the temperatures associated with Figure 34. Note the large lateral temperature gradients associated with this flow which are apparently responsible for the two large circulation patterns which extend nearly the length of the chamber. The small adverse axial gradients associated with this flow tend to support this supposition. Further tests, using many more thermistors in the chamber, are needed to determine the exact relation between these types of gradients.

Figure 30. Zero power flow with adverse axial gradient.

TABLE 13. CHAMBER TEMPERATURES AND TEST PARAMETERS FOR FIGURE 30

Temperatures (°C)			Transverse Temperature Differences (°C)	Lateral/Axial ΔT (°C)			Chamber Parameters
Position	Wall	Center Plane		Span	Wall	Center Plane	
1	21.78	21.68	-0.1	1-2	-0.02	-0.02	T_1 21.3°C
2	21.81	21.7	-0.11	2-3	-0.01	0	T_2 22.1°C
3	21.83	21.7	-0.12	3-8	-0.06	-0.07	T_3 22.1°C
4	21.85	21.78	-0.07	3-6	-0.1	-0.09	
5	21.89	21.82	-0.07	3-4	-0.05	-0.02	Power: 0 W
6	21.92	21.88	-0.04	4-5	-0.02	-0.04	Flow: 19 ml/min
7	21.98	21.98	-0	5-7	-0.09	-0.09	Re no.: 3.5
8	21.9	21 87	-0.03	5-9	-0.1	-0.1	Gr no.: 4.7
9	21.99	21.96	-0.03				Ra no.: 0.8

Figure 31. Initiation of flow disturbance at zero power.

Figure 32. Reverse flow disturbance at zero power.

TABLE 14. CHAMBER TEMPERATURES AND TEST PARAMETERS FOR FIGURE 32

Temperatures (°C)			Transverse Temperature Differences (°C)	Lateral/Axial ΔT (°C)			
Position	Wall	Center Plane		Span	Wall	Center Plane	Chamber Parameters
1	21.9	21.8	0.1	1-2	-0.11	-0.11	T_1 21.8°C
2	22.02	21.92	-0.1	2-3	-0.09	-0.07	T_2 22.7°C
3	22.12	21.99	-0.13	3-8	-0.22	-0.32	T_3 22.7°C
4	22.16	22.08	-0.08	3-6	-0.29	-0.37	
5	22.24	22.15	-0.09	3-4	-0.06	-0.11	Power: 0 W
6	22.39	22.35	-0.04	4-5	-0.07	-0.06	Flow: 19 ml/min
7	22.51	22.5	-0.01	5-7	-0.28	-0.35	Re no.: 3.5
8	22.35	22.3	-0.05	5-9	-0.3	-0.33	Gr no.: 5.6
9	22.54	22.49	-0.05				Ra no.: 2.5

Figure 33. Development of circulations at zero power.

TABLE 15. CHAMBER TEMPERATURES AND TEST PARAMETERS FOR FIGURE 33

Temperatures (°C)			Transverse Temperature Differences (°C)	Lateral/Axial ΔT (°C)			Chamber Parameters
Position	Wall	Center Plane		Span	Wall	Center Plane	
1	21.94	21.84	0.08	1-2	-0.15	-0.14	T_1 21.4°C
2	22.07	21.98	0.09	2-3	-0.07	-0.05	T_2^1 23°C
3	22.23	22.04	0.14	3-8	-0.75	-0.65	T_3^2 23°C
4	22.25	22.18	0.07	3-6	-0.8	-0.75	
5	22.36	22.27	0.1	3-4	-0.2	-0.16	Power: 0 W
6	22.7	22.66	0.05	4-5	-0.15	-0.09	Flow: 19 ml/min
7	22.85	22.82	0.02	5-7	-0.7	-0.61	Re no.: 3.5
8	22.65	22.7	0.04	5-9	-0.65	-0.55	Gr no.: 6.1
9	22.89	22.81	0.06				Ra no.: 4.2

Figure 34. Onset of unstable flow.

TABLE 16. CHAMBER TEMPERATURES AND TEST PARAMETERS FOR FIGURE 34

Temperatures (°C)			Transverse Temperature Differences (°C)	Lateral/Axial ΔT (°C)			Chamber Parameters
Position	Wall	Center Plane		Span	Wall	Center Plane	
1	22.28	22.16	0.12	1-2	-0.01	0	T_1 21.4°C
2	22.29	22.17	0.12	2-3	-0.22	-0.25	T_2 23.3°C
3	22.51	22.35	0.15	3-8	-0.78	-0.8	T_3 23.3°C
4	22.46	22.36	0.1	3-6	-0.73	-0.7	
5	22.5	22.4	0.11	3-4	0.03	0.01	Power: 0 W
6	23.23	22 17	0.06	4-5	-0.03	-0.05	Flow: 19 ml/min
7	23.26	22.5	0.05	5-7	-0.76	-0.75	Re no.: 3.5
8	22.3	22.22	0.08	5-9	-0.7	-0.75	Gr no.: 6.6
9	23.21	23.14	0.08				Ra no.: 5.5

V. COMPARISON WITH THEORY

One of the main reasons for carrying out the described experiments was to support theoretical work done by D. A. Saville [3]. Saville characterized buoyancy-induced disturbances as being superimposed on a symmetric base flow. The disturbance flow $\hat{u}$ and temperature $\hat{\theta}$ were obtained from the perturbation Navier-Stokes and energy equations which are, respectively,

$$\frac{Gr}{Re}\,\hat{\theta} + \nabla^2\hat{u} = 0 \tag{1}$$

$$\frac{RaRe}{Gr}\,\hat{u} = \nabla^2\hat{\theta} \tag{2}$$

where the dimensionless parameters are given in the Appendix. Combining the preceding equations gives

$$\begin{aligned} \nabla^4\hat{u} &= Ra\,\hat{u} \\ \hat{\theta} &= Ra^{-1}\nabla^2\hat{u} \quad . \end{aligned} \tag{3}$$

The solutions to these equations can be written

$$\hat{u} = u_1 + u_2$$

where

$$\nabla^2 u_1 = \lambda^2 u_1$$

and

$$\nabla^2 u_2 = -\lambda^2 u_2 \quad .$$

The general solutions to equation (3) are

$$u_1 = \sin qz(A_1 \sinh \gamma_1 y + B_1 \cosh \gamma_1 y)$$

$$+ \cos qz(A_2 \sinh \gamma_1 y + B_2 \cosh \gamma_1 y)$$

$$u_2 = \sin qz(A_3 \sinh \gamma_2 y + B_3 \cosh \gamma_2 y) \qquad (4)$$

$$+ \cos qz(A_4 \sinh \gamma_2 y + B_4 \cosh \gamma_2 y)$$

where

$$\gamma_1^2 = q^2 + \lambda^2 \quad \text{and} \quad \gamma_2^2 = q^2 - \lambda^2 \quad .$$

The constants are determined by satisfying the no-slip conditions on the chamber walls. The solutions will be either antisymmetric or symmetric with respect to the x-y plane.

Saville found that the antisymmetric mode with the lowest critical Rayleigh number corresponds to the velocity field of

$$\hat{u}_1 = A(x) \sin \frac{\pi z}{H} \cos \frac{\pi y}{2} \quad , \qquad (5)$$

with the critical Rayleigh number of

$$Ra_c = \frac{\pi^4}{16} (1 + 4H^{-2})^2 \quad , \qquad (6)$$

where H is the ratio of chamber width to thickness. The preceding solution is antisymmetric with upflow on one side and downflow on the other. For the chamber tested, $Ra_c = 6.57$.

Several of the test runs have Rayleigh numbers near the preceding value. Consider the results of Table 5 and the flow shown in Figure 22. There appears to be a retardation of flow on the left side of the chamber — a condition characteristic of the antisymmetric mode of equation (5).

The symmetric base flow can be expressed, according to Saville, by

$$u(y,z) = \frac{8}{\pi^3} \sum_0^\infty \frac{k}{n^3} [1 - (-1)^n] \left[\frac{\cosh \frac{n\pi z}{2}}{\cosh \frac{n\pi H}{2}} - 1 \right] \sin \frac{n\pi}{2}(1 + y) \tag{7}$$

where

$$k = \frac{\pi^4 H}{16 \sum_0^\infty \frac{[1-(-1)^n]}{n^4} \left(\frac{2}{n\pi} \tanh \frac{n\pi H}{2} - H \right)} .$$

If we assume A(1.02) = 2 and superimpose equation (5) on the symmetric base flow, we obtain the velocity distribution given in Figure 35. Here A(1.02) is an arbitrary amplitude of the antisymmetric mode at x = 1.02, so that relative amplitudes of disturbance flow to base flow are:

$$\frac{A(1.02)}{u(0,0)} = \frac{2.0}{1.6} = 1.25.$$

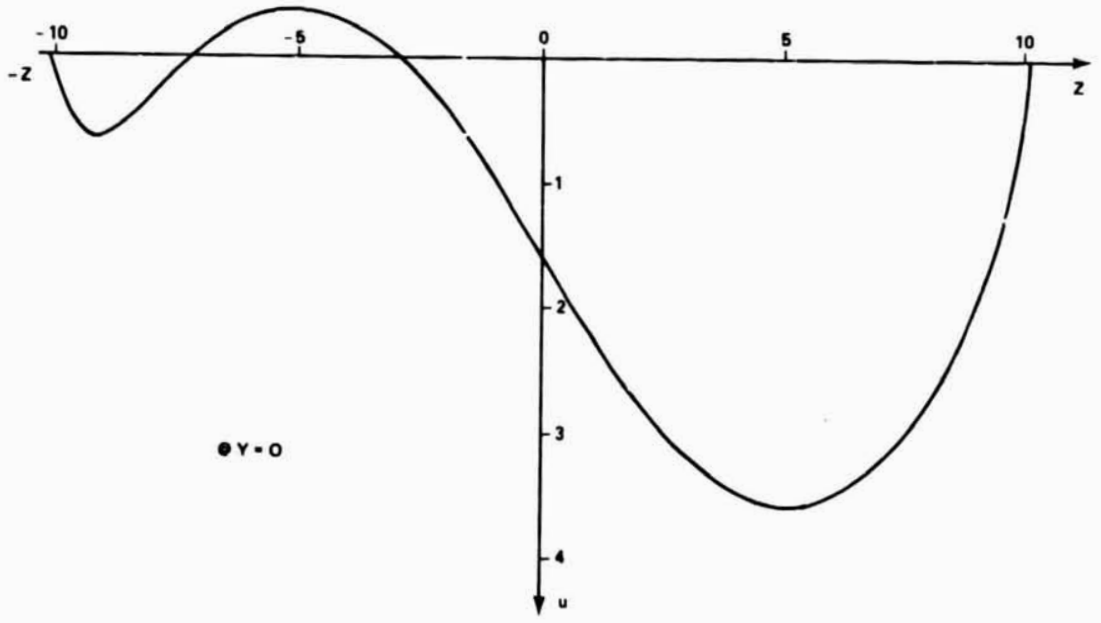

Figure 35. Superposition of antisymmetrical flow disturbance on the base flow.

It is very interesting to note that the velocity distribution at thermistor 4 in Figure 22 shows this exact velocity distribution. In particular, note the downflow at the left side wall, the diffused conditions of streams b and c at the left center and right center of the chamber, and the region of high downflow on the right. Figure 35 shows the downflow on the extreme left, a region of high shear at the center, and high downflow on the right.

Note also a similar region of flow perturbation at thermistor 2 in Figure 22. This disturbance is caused by the adverse temperature gradient between thermistors 1 and 2. The gradient is not sufficient, however, to cause backflow, but does cause the deflection of stream b due to the retarded flow on the left side of the chamber — in agreement with the conditions predicted by equation (5).

That the previously discussed velocity redistribution in the chamber does produce the observed deflection has been shown experimentally in Figure 14. Here the velocity profile was modified by inducing a fluid leak which produces the same type of velocity field as shown in Figure 22 and as depicted by equation (5).

A very explicit example of the previous antisymmetric disturbance is shown in Figure 27. These flows can be described by superposition of equation (5) on the symmetric base flow. The flow patterns are on opposite sides of the chamber and are caused by the adverse temperature gradients indicated in Table 10. They are separated by a region of stable flow between thermistors 2 and 3 which is verified by ∇T_{2-3} in Table 10. Indeed, the presence of the essentially neutral gradient ∇T_{2-3} allows these patterns to be formed next to each other.

Figure 25 shows stream a in a region of downflow near the left side wall at $z = -9$, while the maximum downflow on the left in Figure 35 occurs at $z = -8.5$. Streams b and c are in a region of high shear, as also depicted by the velocity distribution of Figure 35. Streams d and e, conversely, are in a region ($z = 7$ to 10) of high downflow, again in agreement with the velocity distribution of Figure 35.

Flow disturbances produced by adverse lateral gradients (as in Figure 29) produce up flow at the wall. Therefore, it is obvious from the flows observed that localized heating on the side walls is responsible for these disturbances.

The flows generated in the zero power runs (Figs. 31 through 34) are the result of localized adverse gradients but are too unstable to be directly linked to the particular disturbance modes given previously. The Rayleigh numbers (Tables 15 and 16), however, are in agreement with the critical values predicted by the theory, while the initial disturbance patterns shown in Figure 31 appear to be due to adverse lateral gradients as indicated by Table 14.

VI. CONCLUSIONS

Disturbances to the symmetric base flow begin when local adverse axial temperature gradients are formed in the chamber. The effect of these gradients is to retard or increase local flow velocities at different positions in the chamber cross section, which results in lateral secondary flows being induced in the chamber. These secondary flows exhibit themselves as deflections and/or distortions of the sample streams. As the adverse axial gradients increase in magnitude and the critical Rayleigh number is approached, reverse flow is apparent, which subsequently leads to the onset of unstable flow.

Other, similar disturbances occur at the chamber side walls as the result of adverse lateral temperature gradients. Indeed, the criteria which determine whether a disturbance is produced by a lateral gradient or an axial gradient appear to be the flow conditions observed along the chamber side walls. If we consider an adverse lateral gradient and compare the local temperature along a level (i.e., in the x-z plane) to the average temperature in the level, then we would expect to see upward induced buoyancy flows next to the wall.

Preliminary tests on the phase II chamber indicate that upflow of the buffer may be desirable from heat exchanger considerations. It was observed that co-flow of the buffer and coolant gave a much larger favorable axial gradient than that associated with counterflow cooling. Also, the co-flow (upflow of the buffer) configuration did not show the development of an adverse axial gradient in the vicinity of thermistor 4 as in the case of counterflow cooling (downflow of the buffer); however, an adverse axial gradient did develop at the top of the chamber, as would be expected.

Further tests are planned to (1) develop fully the temperature and velocity fields, (2) operate the chamber at different orientations of the gravity vector, and (3) complete the upflow experiments.

Qualitatively, the reduction in stable gradients, both axial and lateral, signals the degradation of the uniform base flow which is vital to the electrophoresis process. Also, it is consistent throughout the results that the presence of adverse gradients indicates that the flow has been seriously degraded with large deflections and/or circulations.

APPENDIX

The dimensionless parameters given in the tables are calculated using the following expressions:

$$Re = \frac{Vd}{\nu}$$

$$Gr = \frac{g\beta\ \Delta T\ d^3}{\nu^2}$$

$$Ra = \frac{g\beta\ A\ d^4}{\nu\alpha}$$

where V is the average throughput velocity; d is the chamber half thickness; ν is the fluid viscosity evaluated at the chamber average temperature; β is the coefficient of thermal expansion evaluated at the chamber average temperature; ΔT is the maximum transverse ΔT along the chamber center line; A is the maximum adverse axial gradient in the chamber; and α is the thermal diffusivity evaluated at the chamber average temperature.

Tables 1 through 16 give the thermistor temperatures at positions 1 through 9. The temperatures are recorded both at the wall and at the center plane of the chamber, with the transverse temperatures being the difference between these values. The lateral gradients are taken between spans 3-8, 3-6, 5-7, and 5-9, while the axial gradients are 1-2, 2-3, 3-4, and 4-5. Positive values are favorable gradients, while negative values are adverse gradients. T_1 is the buffer inlet temperature, while T_2 and T_3 are the coolant entrance and exit temperatures, respectively.

REFERENCES

1. Ostrach, S.: The Influence of Convection in Continuous Flow Electrophoresis. ESA Special Publication 114, 1976.

2. Semon, H. W.: Investigations of Flow Stability in the SPAR Wide-Gap Electrophoretic Separator Chamber. Report for NASA, MSFC by GE Space Sciences Laboratory, Philadelphia, Pennsylvania, 1977.

3. Saville, D. A. and Ostrach, S.: Fluid Mechanics of Continuous Flow Electrophoresis. NASA Contract NAS8-31349, Universities Space Research Association, Houston, Texas, 1978.

APPROVAL

SAMPLE STREAM DISTORTION MODELED IN CONTINUOUS-FLOW ELECTROPHORESIS

The information in this report has been reviewed for technical content. Review of any information concerning Department of Defense or nuclear energy activities or programs has been made by the MSFC Security Classification Officer. This report, in its entirety, has been determined to be unclassified.

ROBERT S. SNYDER
Chief, Separation Processes Branch

ROBERT J. NAUMANN
Chief, Space Processing Division

CHARLES A. LUNDQUIST
Director, Space Sciences Laboratory